are weak H_3^+ lines around 4.14 μm, the CVF bandpass completely smooths out the narrow lines. We therefore see a relatively dark pole, due to limb darkening, as shown in Fig. 1*a*. From the relative line intensities of H_3^+ in the spectrum of Fig. 2*b*, a rotational temperature of 950 ± 100 K is derived. This is nominally lower than, but still consistent with, the temperature (1,100 ± 100 K) measured from 2-μm H_3^+ emission in 1988.

In the first row of Fig. 3, we present a time sequence of three north polar images in the 3.53-μm band, which is one of the most sensitive to H_3^+ emission, showing variation of the H_3^+ hot-spot feature as the planet rotates. In particular, the second image was taken at a CML of 185°, and shows no significant brightening at this longitude. A northern hot spot has been observed near 180° in the ultraviolet and at 7.8 μm over the past 10 years (ref. 3), and it was present at the same longitude on 7 and 8 March (UT) in the ultraviolet, according to the IUE observations (R. Prange, personal communication). The second row of Fig. 3 presents a time sequence of southern hot-spot images. Intensity variations are clearly seen in this sequence. Limb brightening is observed when the H_3^+ hot spot is close to the limb.

The three images in Fig. 4 were taken in a 10-min interval on 8 March, at wavelengths of 3.50, 3.37 and 3.29 μm, near the centre of the ν_3 band of methane, where we expect strong absorption by methane but only weak emission from H_3^+ (no FTS spectra were obtained at these wavelengths). In the images, however, there is a very bright area. The hot-spot intensity in the third image is ~10 times as great as that of the rest of the planet. The absolute intensity at the emission peak of the third image in Fig. 4 is roughly the same as those of images in Fig. 3, which were taken on 7 March. All ProtoCAM images and FTS spectra, however, show a decrease in overall intensity of polar brightening by at least a factor of 3 on the second day. As we were not able to detect strong H_3^+ emission lines in the 3.4–4.2 μm range at that time, we do not expect that high-J rotational H_3^+ lines were strong near 3.3 μm. We suggest that methane line emission from the upper stratosphere in the auroral zone, where temperatures are high, may be partly responsible for this bright emission. Reflection of infrared sunlight by the polar haze may also contribute, because the continuum morphology is similar to that of polar haze previously observed[9] at 2 μm.

We constructed a methane emission model using existing models[10,11] and carried out a line-by-line calculation of radiative transfer, including methane absorption in the Earth's atmosphere and a jovian radial Doppler shift. We found that most of the emission of the 3-μm band of methane originates from roughly the 10-μbar level, where temperatures are 300–400 K. The calculated intensity variation at the mean wavelengths of the images near the methane band is roughly consistent with the observed intensity variation, within a factor of two. Before we can unambiguously confirm or exclude the possibility of emission from the methane in the auororal zone, further FTS observations at high spectral resolution are needed. □

Received 16 April; accepted 23 August 1991.

1. Broadfoot, A. L. *et al. Science* **204,** 979–982 (1979).
2. Clarke, J. T., Moos, H. W., Atreya, S. K. & Lane, A. L. *Astrophys. J.* **241,** L179–L182 (1980).
3. Caldwell, J., Tokunaga, A. T. & Gillett, F. C. *Icarus* **41,** 667–675 (1980).
4. Drossart, P. *et al. Nature* **340,** 539–541 (1989).
5. Oka, T. & Geballe, T. R. *Astrophys. J.* **351,** L53–L56 (1990).
6. Miller, S., Joseph, R. D., & Tennyson, J. *Astrophys. J.* **360,** L55–L58 (1990).
7. Maillard, J.-P., Drossart, P., Watson, J. K., Kim, S. J., & Caldwell, J. *Astrophys. J.* **363,** L37–L41 (1990).
8. Baron, R. L. & Owen, T. *IAU Circ.* No. 5132 (8 *November*, 1990).
9. Kim, S. J. *et al. Icarus* **91,** 145–153 (1991).
10. Kim, S., Drossart, P., Caldwell, J. & Maillard, J.-P. *Icarus* **84,** 54–61 (1990).
11. Kim, S., Kratz, D. & Halthore, R. *EOS Trans. Am. geophys. Un.* **72,** 236 (1991).
12. Gezari, D. Y., Schmitz, M. & Mead, J. M. *Catalog of Infrared Observations. Part I—Data, 2nd Ed., NASA Ref. Publ.* 1196 (1987).

ACKNOWLEDGEMENTS. The modified temperature–pressure profile used here was constructed with the help of D. Kratz and R. Halthore. We thank F. Lacombe for help with image processing.

Imaging Jupiter's aurorae from H_3^+ emissions in the 3–4 μm band

Richard Baron*, Robert D. Joseph*, Tobias Owen*, Jonathan Tennyson†, Steven Miller†, & Gilda E. Ballester‡

* Institute for Astronomy, University of Hawaii, 2680 Woodlawn Drive, Honolulu, Hawaii 96822, USA
† Department of Physics and Astronomy, University College London, Gower Street, London WC1E 6BT, UK
‡ Department of Earth Sciences, University of Oxford, Parks Road, Oxford OX1 3PR, UK

SINCE H_3^+ was first spectroscopically detected on Jupiter[1,2], there has been considerable interest in using this simple molecular ion to probe conditions existing in the planet's auroral regions. Here we present a series of images of Jupiter recorded at wavelengths sensitive to emission by H_3^+, which reveal the spatial distribution of excited H_3^+ molecular ions in the jovian ionosphere, as seen from Earth. We believe that they provide high-spatial-resolution images of polar aurorae on Jupiter. They suggest that the intensity of the auroral emission can vary on a timescale of an hour, a shorter period than had previously been noted. We also find that the spatial distribution of H_3^+ emissions correlates only partially with the loci of auroral activity inferred from ultraviolet and longer-wavelength infrared observations. The H_3^+ emission may therefore be controlled by auroral processes that are different from those responsible for the ultraviolet and infrared emissions.

The molecular ion H_3^+ is produced in the jovian ionosphere at high latitudes by the ionization of H_2 resulting from charged particle precipitation from the magnetosphere; the rapid reaction of H_2^+ and H_2 produces H_3^+ (ref. 1). In subsequent reactions, H_3^+ can provide both hydrogen atoms and protons, which can initiate complex hydrocarbon chemistry when produced below the homopause[2], making it a sensitive probe of energy deposition from the magnetosphere into the atmosphere by high-energy particles.

Infrared emission from H_3^+ was first detected on Jupiter in 1988 in the 2-μm K window by the measurement of 23 lines of the $2\nu_2(l=2)\rightarrow 0$ overtone band[1,3], and identified from

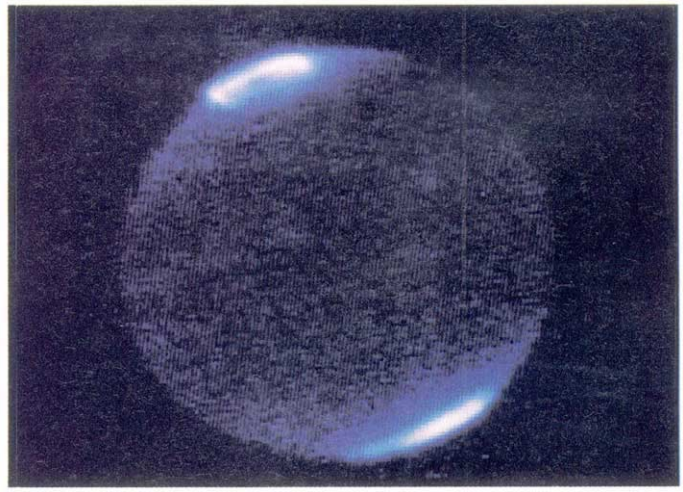

FIG. 1 Mosaic of nine ProtoCAM images of Jupiter measured at 3.40 μm at ~1% spectral resolution. Each frame had an effective integration time of 40 s. The detector in ProtoCAM is a 58 × 62 InSb array. The equatorial diameter of Jupiter subtended 45.7 arcsec and the polar diameter 42.7 arcsec. The most intensive areas are shown as pink to white, and the least intense as dark blue to black. The System III CML of this image is 163°.

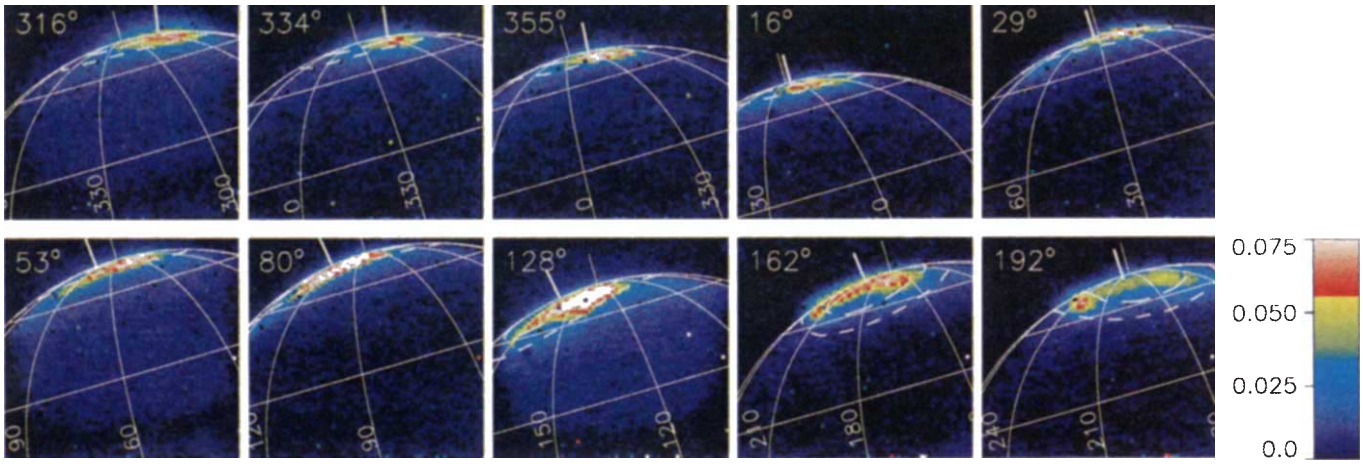

FIG. 2 Images of Jupiter's north polar region measured at 3.55 μm on 24 February 1991. The CML for each image is indicated on the top-left corner. The planetary 'surface' fitted to each image is shown, corresponding to polar radius of 20.8 arcsec, equatorial radius of 22.25 arcsec, sub-Earth latitude of 0.4° and north pole position angle of 16°. Lines of latitude and longitude are shown at 30° intervals. The spin axis is indicated by a thin line, and the magnetic axis, offset from the spin axis of the planet by ~10° towards longitude 202° in the north, is indicated by a thick line. Also shown is the ultraviolet auroral oval (dashed lines) as determined from Voyager, as well as an estimated oval displaced by 9° towards the magnetic pole (dotted-dashed lines) to represent precipitation from near the magnetotail. The colour scale is linear, ranging from 0.0 to 0.075 erg cm^{-2} s^{-1} $sterad^{-1}$. Some images show saturation in this scale (the actual intensities can be as large as 0.12 erg cm^{-2} s^{-1} $sterad^{-1}$).

calculated frequencies and Einstein A_{if} coefficients in conjunction with laboratory spectra[4]. Since then, the H_3^+ fundamental $v_2 \rightarrow 0$ spectrum has been measured in Jupiter, showing that the upper emitting levels are being populated thermally[5]. Other studies indicate that the temperature of the emitting gas is not constant in time and that there are variations in the relative strengths of the emissions in the northern and southern auroral zones[6,7].

Baron and Owen[8] first obtained images of Jupiter at a wavelength sensitive to H_3^+ in January 1991, using ProtoCAM, the infrared camera on the NASA 3-m Infrared Telescope Facility (IRTF). This camera incorporates three circular variable filters (CVFs) with spectral resolutions that are ~1–2% of the bandpass (full width at half minimum). These three CVFs cover the wavelength range from 1.3 to 5.5 μm. Here we present new images obtained on the nights of 1 and 22–24 February 1991,

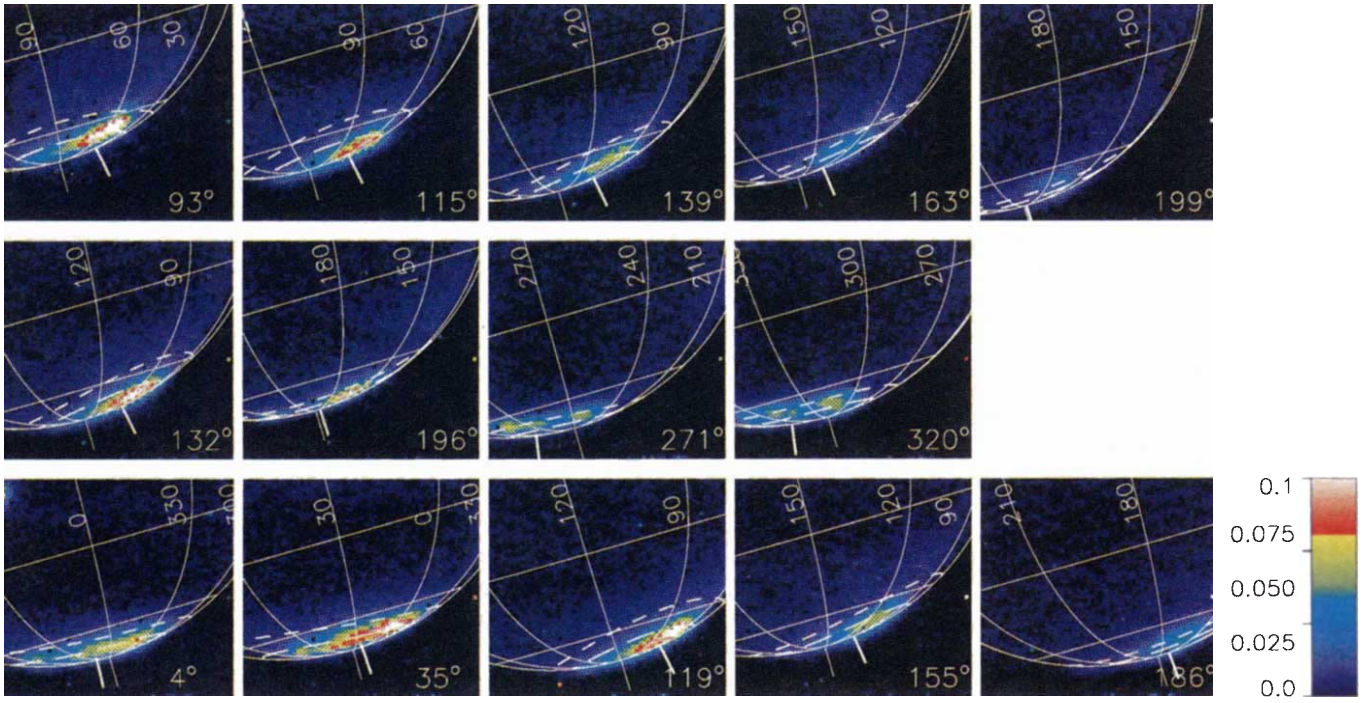

FIG. 3 Images of Jupiter's south polar region measured at 3.4 μm for the nights of 22 February (top row), 23 February (middle row) and 24 February (bottom row). Theoretical auroral ovals mapped by the Io plasma torus (dashed lines) and the magnetotail (dotted-dashed lines) are shown. The linear colour scale ranges from 0.0 to 0.100 erg cm^{-2} s^{-1} $sterad^{-1}$, and as in Fig. 2, some images show saturation in this scale.

Hawaii Standard Time. The image scale was 0.35 arcsec per pixel and the seeing on all nights except 24 February was <1 arcsec; on 24 February it was ~1.5 arcsec. The tracking during a single image acquisition was better than 0.1 arcsec. Although we made observations throughout the 1-5-μm spectral range (S.M. *et al.*, manuscript in preparation), we are concentrating here on the interpretation of images obtained in the L window at 3.4 and 3.55 μm. At the ~1% CVF resolution, these wavelengths correspond to strong H_3^+ features formed by the merging of a number of R-branch transitions of $v_2 \rightarrow 0$. The P branch of v_3 of methane also occurs in this wavelength range.

Figure 1 is a mosaic of nine reduced ProtoCAM frames (sky-subtracted, flattened and bad pixels removed) taken on 1 February, with the CVF centred on 3.4 μm, to form a composite image of Jupiter. We attribute the overall darkness of the planet to the absorption of incident solar radiation by stratospheric methane. Bright emission features are evident at the poles of the planet, and we interpret these as being mainly due to H_3^+ emission. To support this interpretation, we looked at various sequences of polar images at wavelengths throughout the L window. After compensation has been made for the effects of absorption by the Earth's atmosphere, the relative intensities of the peak polar emission correlate well with the expected H_3^+ spectrum (S.M. *et al.*, manuscript in preparation). In contrast, the observed intensities do not follow the v_3 spectrum of methane, although emission from this molecule around 7.8 μm has been observed in the auroral zones[9]. The contribution of continuum around the poles was estimated from the flux we measured at 3.8 μm (S.M. *et al.*, manuscript in preparation), which corresponds to a null in the H_3^+ emission spectrum. The maximum emission at this wavelength was found to be ~0.025 erg cm^{-2} s^{-1} $sterad^{-1}$, about 20% of the maximum northern emission at 3.55 μm on 24 February, corresponding roughly to the boundary between dark and light blue on the saturated colour scale in Fig. 2. Emission above this level is therefore considered to be due to H_3^+.

Figure 2 shows a sequence of ProtoCAM frames taken at the jovian north pole at 3.55 μm on 24 February 1991. Figure 3 shows similar sequences measured at 3.4 μm in the southern hemisphere on 22, 23 and 24 February 1991. Central meridian longitudes (CML) in magnetic longitude system III are indicated. To aid interpretation, we have fitted the planet's oblate 'surface' at the time of the observation to each image to within ±0.5 arcsec, using the low-level signal from the limbs in regions away from the H_3^+ emission. This was accomplished by comparing the individual frames by eye with a full mosaic of the planet to which a calculated disk had been reliably fitted. The fitted mosaic shows slight limb darkening of the reflected continuum at low latitudes, which increases towards the poles. The H_3^+ emissions are optically thin[1] and must show some limb brightening. Although extensive modelling would therefore be required to extract detailed quantitative information from the images, some general time-dependent and morphological characteristics can still be determined.

Comparison of the north polar images taken at CML 128° and 162° on 24 February indicates that the observed average emission between longitudes 135° and 155° and latitudes 65° and 75° weakened by ~25% during the hour between the images (Fig. 2). As this region has the same geometric aspect on both images, the differences in its intensity should not be due to limb brightening effects. Additionally, if we assume the morphology of the emission apparent in the image at 128° is maintained in the image at 162°, line-of-sight effects would cause the emission in the latter image to appear brighter, in contrast to what is observed. We therefore believe the most reasonable explanation of this effect is that it corresponds to an actual intensity variation of ~25% taking place in the jovian atmosphere during the hour between the two images. In the absence of detailed modelling, however, some contribution from geometric effects cannot be ruled out entirely. On the same night, strong emission at the southern pole appears to grow between longitudes 330° and 60° in the hour between the images taken at CML 4° and 35° (Fig. 3, bottom row). Variation in emission strength among the three nights was also noted on both poles. For example, images taken on 22 February at CML 139° and on 23 February at 132° indicate that the southern emission was stronger on 23 February. Other data show that the north pole was also brightest on 23 February.

We have attempted to correlate the basic morphology of the H_3^+-emitting regions with that reported for the ultraviolet-H_2 and infrared-hydrocarbon aurorae, whose connection has not yet been determined. For the northern hemisphere (Fig. 2), we have plotted the loci of diffuse ultraviolet-H_2 auroral emissions as determined by the ultraviolet experiments on the Voyager missions[10,11] in 1979. It has been suggested[12] that this oval may be related to magnetospheric precipitation from the neighbourhood of the Io plasma torus. In addition, we have plotted an estimated oval displaced by 9° towards the magnetic pole to represent precipitation from regions further out towards the magnetotail. In the absence of Voyager data for the southern images we have plotted theoretical ultraviolet auroral ovals mapped by the torus and the magnetotail based on the O_4 plus current-sheet magnetic field model[13,14]. A peak in the northern ultraviolet emission at longitude 180° was detected by Voyager[10,11] and subsequent ultraviolet observations with the IUE satellite[15], although recent IUE observations (of relatively poor spatial resolution) have also shown unusual longitudinal intensity distributions[16]. The south ultraviolet peak varies around longitude 20° (ref. 17). The infrared-hydrocarbon aurora[9,18-21] has been most extensively studied in its methane emission which consists of areas of high-level emission, possibly thermally excited, known as 'hot spots'. These occur at latitudes 60° in the northern hemisphere and ~70° in the south, and seem to be fixed in the north at longitude 180°, close to the ultraviolet peak, whereas their location in the south varies considerably in the region 300°-90° (refs 9, 18).

Our observations indicate that in both hemispheres, the regions of H_3^+ emission are fixed with respect to the magnetic pole and are confined to latitudes above 60°, extending over the entire polar region. This extent of the emitting region is in agreement with recent detailed mapping of the 4.0-μm spectrum of Jupiter (S. Ridgway *et al.*, manuscript in preparation). In the north (Fig. 2), the emissions show relatively bright spots centred around longitudes ~145° and ~230°. A local minimum occurs around longitude 180°. These features can be seen rising and setting in the sequence shown. Although we present results for only one night for the northern hemisphere, we observed similar morphology on the other two nights. The structure of the H_3^+ emission region in the south is more complex (Fig. 3), due in part to the apparent temporal variations noted above. Taking the three nights together, strong emissions are seen from longitude 300° to 90°, with an additional weak maximum at ~260°.

We conclude that the observed H_3^+ emission does not correspond exactly to any of the auroral ovals described above. This is particularly striking at 180° longitude in the north, where the peak of the ultraviolet auroral emission is usually observed, as is the methane hot spot. In the south, the overall longitudinal region of the methane emission as well as that of the ultraviolet emission seems to coincide with that of the H_3^+ emission, but more detailed, time-resolved comparisons are required.

Further studies of the jovian ionosphere in the auroral regions are required to provide mechanisms to explain the basic results presented here. The possibility that the H_3^+ emissions are controlled to some extent by auroral processes[12] different from those responsible for the ultraviolet and infrared-hydrocarbon emissions has to be explored. But a proper assessment of the relation of the various types of auroral emissions can only be made after detailed modelling of the dependence of the emissions on variables that may vary spatially, such as the atmospheric level at which the incoming magnetospheric particles deposit energy[15], and that may affect the different types

of emissions in different ways. Nevertheless, our preliminary results clearly demonstrate that infrared spectral imaging provides a powerful tool for jovian auroral studies, permitting measurements of the spatial extent and temporal variations of auroral activity on Jupiter at sub-arcsec angular resolution. Concurrent data on H_3^+ and methane as well as H_2 emissions would be extremely helpful, as well as observations to determine just how rapidly the variations noted in H_3^+ emission strength occur. Such data, combined with other measurements, will provide a strong constraint on physical, chemical and dynamical models of the jovian system. □

Received 29 May; accepted 22 August 1991.

1. Drossart, P. *et al Nature* **340,** 539–541 (1989).
2. Strobel, D. F. *Int. Rev. Phys. Chem.* **3,** 145–176 (1983).
3. Trafton, L., Lester, D. F. & Thompson, K. L. *Astrophys. J.* **343,** L73–L76 (1989).
4. Majewski, W. A. *et al. Astrophys. J.* **347,** L51–L54 (1989).
5. Miller, S., Joseph, R. D. & Tennyson, J. *Astrophys. J.* **360,** L55–L58 (1990).
6. Oka, T. & Geballe, T. R. *Astrophys. J.* **351,** L53–L56 (1990).
7. Maillard, J.-P., Drossart, J., Watson, J. K. G., Kim, S. J. & Caldwell, J. *Astrophys. J.* **363,** L37–L40 (1990).
8. Baron, R. & Owen, T. *IAU Circ. No.* 5132 (1990); *IAU Circ. No.* 5211 (1991).
9. Caldwell, J., Tokunaga, A. T. & Gillett, F. C. *Icarus* 44, 667–675 (1980).
10. Broadfoot, A. L. *et al. J. geophys. Res.* **86,** 8259–8284 (1981).
11. Herbert, F., Sandel, B. R. & Broadfoot, A. L. *J. geophys. Res.* **92,** 3141–3154 (1987).
12. Prangé, R. *Adv. Space Res.* (in the press).
13. Connerney, J. E. P., Acuña, M. H. & Ness, N. F. *J. geophys. Res.* **86,** 8370–8384 (1981).
14. Skinner, T. E. thesis, Johns Hopkins Univ. (1984).
15. Livengood, T. A., Strobel, D. F. & Moos, H. W. *J. geophys. Res.* **95,** 10365–10373 (1990).
16. Livengood, T. A., Prangé, R., Ballester, G. E. & Moos, H. W. *EOS* **72,** 186–193 (1991).
17. Livengood, T. A. & Moos, H. W. *Geophys. Res. Lett.* **17,** 2265–2268 (1990).
18. Caldwell, J., Halthorne, R., Orton, G. S. & Bergstrahl, J. *Icarus* **74,** 331–339 (1988).
19. Drossart, P. *et al. Icarus* **66,** 610–618 (1986).
20. Kostiuk, T., Espenak, F., Mumma, M. J. Deming, D. & Zipoy, D. *Icarus* **72,** 394–410 (1987).
21. Kim, S. J., Caldwell, J., Rivolo, A. R. & Wagener, R. *Icarus* **64,** 233–248 (1985).

ACKNOWLEDGEMENTS. We acknowledge the assistance of the IRTF telescope operators W. Golisch and C. Kaminski. We also thank R. Prangé and T. Livengood for conversations. J.T. was a visiting astronomer at the IRTF, which is operated by the University of Hawaii under contract to NASA. J.T. and S.M. acknowledge support from the UK SERC.

Local oxygen ordering in superconducting $YBa_2Cu_3O_{6.4}$ observed by neutron diffraction

Thomas Zeiske*, Rainer Sonntag†, Dietmar Hohlwein*† Niels Hessel Andersen‡ & Thomas Wolf§

* Hahn-Meitner-Institut Berlin, W-1000 Berlin 39, Glienicker Straße 100, Germany
† Institut für Kristallographie der Universität Tübingen, Germany
‡ Physics Department, Risø National Laboratory, DK-4000 Roskilde, Denmark
§ Kernforschungszentrum Karlsruhe, ITP, Germany

THE superconducting transition temperature, T_c, in the $YBa_2Cu_3O_{6+x}$ system is known to depend not only on the oxygen stoichiometry[1], but also on the degree of oxygen order[2,3]. Observations of oxygen ordering structures by electron microscopy[4,5] have led to the suggestion that the '60-K plateau' near $x = 0.5$ in the curve of T_c versus x arises from an ordered structure (the 'ortho-II phase') in which Cu–O and Cu chains alternate in the basal plane[6]. Until now, however, the ortho-II phase has been seen only by electron diffraction, except for one observation at an oxygen stoichiometry of $x = 6.7$ by X-ray diffraction[7]. Compared with true bulk methods such as X-ray and neutron diffraction, electron diffraction suffers from the disadvantage that only a very small portion of the sample is probed. Here we report the observation, by neutron diffraction, of local ortho-II ordering in an $YBa_2Cu_3O_{6.4}$ crystal ($T_c = 38$ K). The observed correlation lengths along the principal axes are $24b$ (along the chains), $10a$ and $2c$. Our observation of the existence of the ortho-II phase for an oxygen stoichiometry close to the minimum for which superconductivity is observed ($x \approx 0.4$) supports existing theoretical models[8,9], in particular one[8] that relates T_c to the presence of two types of ordered domain.

In $YBa_2Cu_3O_{6+x}$ superconductivity occurs for $x \geq 0.4$, and T_c increases with increasing oxygen content to 93 K at $x = 1$. The curve has two plateaux, near $x = 1$ ($T_c = 90$) and $x = 0.5$ ($T_c = 60$ K)[1]. The importance of local oxygen ordering for superconductivity in $YBa_2Cu_3O_{6+x}$ was demonstrated in refs 2 and 3, where the increase of T_c as samples were annealed at room temperature was attributed to progressive local ordering of oxygen atoms in the basal plane.

Poulsen *et al.*[8] studied the oxygen ordering in the basal Cu–O planes by computer simulations and its influence on T_c through a simple charge-transfer process. Assuming that only the ordered ortho-I and ortho-II phases (ortho-I: the normal orthorhombic phase for $x = 1$; ortho-II: a phase near the composition $x = 0.5$, consisting of alternating full and empty Cu–O chains) contribute to superconductivity, and that the ordered domains have to be at least a certain size, they could obtain a theoretical prediction of $T_c(x)$ in close quantitative agreement with the two plateaux found experimentally. Their model description of T_c as a function of x is based on the two-dimensional model of anisotropic next-nearest-neighbour interaction (the ASYNNNI model) first introduced by de Fontaine *et al.*[9]. Despite its simplicity, the ASYNNNI model can account in detail[10,11] for many of the most significant experimental results, including the stability of the ortho-II phase, the structural phase boundary between tetragonal disordered and orthorhombic ordered structures[12], and thermodynamic anomalies observed in the oxygen equilibrium pressures[12,13]. But there are experimental observations for which the ASYNNNI model cannot account, such as the ortho-III phase[4], which requires longer-range interactions[14] than were included in the original ASYNNNI model. Another significant result that cannot be accounted for is the superstructure formation in the tetragonal disordered phase, which has been established recently[15] from single-crystal neutron-diffraction studies of a sample with oxygen stoichiometry $x = 0.35$. From the intensities of superstructure reflections a tetragonal oxygen ordering model ($2\sqrt{2}a \times 2\sqrt{2}a \times c$) was derived. In this structure, 'half-filled' Cu–O chains alternate with 'quarter-filled' chains.

The importance of oxygen ordering for superconductivity in $YBa_2Cu_3O_{6+x}$ calls for an increasing knowledge about the oxygen ordered structures in all parts of the phase diagram. Until recently, only the detailed structures of the endmember compounds, $x = 0$ and $x = 1$, could be determined by neutron and

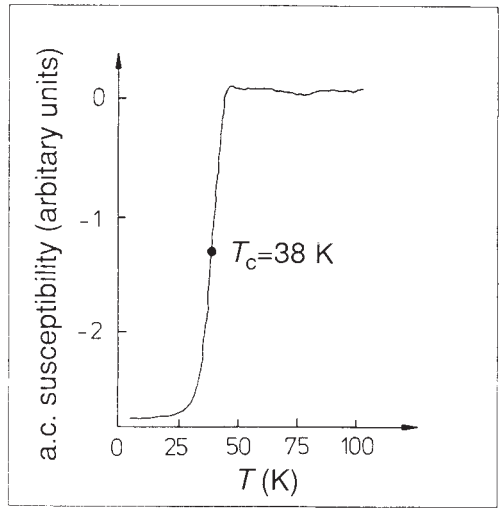

FIG. 1 The a.c. susceptibility curve giving $T_c = 38$ K with a transition width of 5 K.